RAPID COMMUNICATION

Visualizing interface states in In_2Se_3–WSe_2 monolayer lateral heterostructures

Da Huo(霍达), Yusong Bai(白玉松), Xiaoyu Lin(林笑宇), Jinghao Deng(邓京昊), Zemin Pan(潘泽敏), Chao Zhu(朱超), Chuansheng Liu(刘传胜)[†], and Chendong Zhang(张晨栋)[‡]

School of Physics and Technology, Wuhan University, Wuhan 430072, *China*

(Received 30 December 2022; revised manuscript received 8 February 2023; accepted manuscript online 10 February 2023)

Recent findings of two-dimensional (2D) ferroelectric (FE) materials provide more possibilities for the development of 2D FE heterostructure electronic devices based on van der Waals materials and the application of FE devices under the limit of atomic layer thickness. In this paper, we report the *in-situ* fabrication and probing of electronic structures of In_2Se_3–WSe_2 lateral heterostructures, compared with most vertical FE heterostructures at present. Through molecular beam epitaxy, we fabricated lateral heterostructures with monolayer WSe_2 (three atomic layers) and monolayer In_2Se_3 (five atomic layers). Type-II band alignment was found to exist in either the lateral heterostructure composed of anti-FE β'-In_2Se_3 and WSe_2 or the lateral heterostructure composed of FE β^*-In_2Se_3 and WSe_2, and the band offsets could be modulated by ferroelectric polarization. More interestingly, interface states in both lateral heterostructures acted as narrow gap quantum wires, and the band gap of the interface state in the β^*-In_2Se_3–WSe_2 heterostructure was smaller than that in the β'-In_2Se_3 heterostructure. The fabrication of 2D FE heterostructure and the modulation of interface state provide a new platform for the development of FE devices.

Keywords: two-dimensional ferroelectric materials, scanning tunneling microscope, lateral heterostructure, band alignment

PACS: 68.37.Ef, 68.37.–d, 81.15.–z, 79.60.Jv **DOI:** 10.1088/1674-1056/acbaef

1. Introduction

Two-dimensional (2D) materials heterostructures (HSs) play an important role in fields such as field effect transistors,[1] optoelectronic devices,[2] and memory devices[3] due to many fascinating properties, and are an important part of the modern semiconductor industry.[4] On the one hand, the weak interlayer coupling between 2D materials makes it easy to manufacture vertical heterostructures.[5] On the other hand, it is relatively complex to manufacture lateral HSs.[4–6] At present, transition metal dichalcogenides (TMDC) lateral HSs are widely studied,[4,7,8] and another form of lateral HSs with different spatial symmetry,[5] such as hBN-TMDC HSs,[9] graphene-TMDC HSs,[10] also shows unique electronic and optical properties,[11] which are a strong candidate for the next generation of electronic and optoelectronic devices.[12]

Recently, a series of 2D ferroelectric semiconductor materials have been found theoretically and experimentally, such as In_2Se_3[13] and SnTe,[14] which rapidly attract great interest in integrating them into van der Waals (vdW) heterostructures due to their spontaneous reversible polarization. For instance, a ferroelectric field-effect transistor based on MoS_2/$CuInP_2S_6$ 2D vdW HS shows resistance switch characteristics with larger than four on/off ratios between low and high resistance states.[15] Near-infrared (NIR) photodetector-based WSe_2/α-In_2Se_3 heterostructure shows an ultrasensitive characteristic in the NIR wavelength range, due to the ferroelectric gating effect of α-In_2Se_3 enhancing the photodetector detectivity.[16] However, there are few reports on 2D ferroelectric lateral HSs.[5] Lateral HSs are involved in the construction of modern metal-oxide-semiconductor field-effect transistors, which have broad application prospects due to their potential development and tuning degrees of freedom.[5] In addition, the interface of lateral HS is also an excellent platform for studying interfacial electronic structures of materials.[8,17] Therefore, it is an appealing task to study 2D ferroelectric lateral HSs for the development of electronic devices.

Here, we report the ultrahigh vacuum-molecular beam epitaxy (UHV-MBE) growth and scanning tunneling microscopy (STM) characterization of the lateral HS between three atomic layers monolayer (ML) semiconductor WSe_2 and five atomic layers ML ferroelectric semiconductor In_2Se_3. We showed a type-II band alignment between WSe_2 and In_2Se_3 (for both the β' and β^* phases) by scanning tunneling spectroscopy (STS), and the band offsets could be modulated by the ferroelectric polarization of β^*-In_2Se_3. In addition, we discovered the existence of interface states with narrow gaps as interface quantum wires. More interestingly, we observed that the gap size of the interface state in In_2Se_3–WSe_2 lateral HS was different (0.62 eV and 0.45 eV in the β'/β^*-In_2Se_3–

[†]Corresponding author. E-mail: csliuan@whu.edu.cn
[‡]Corresponding author. E-mail: cdzhang@whu.edu.cn

© 2023 Chinese Physical Society and IOP Publishing Ltd

WSe_2 HS, respectively), the ferroelectric polarization can be an effective toolset tuning the gap size of the interface states. Our findings provide a new approach for the fabrication of 2D ferroelectric lateral HS and the modulation of electronic states at the interface.

2. Experimental methods

The lateral HS was grown on bilayer graphene (BLG)/SiC substrate using a home-built ultrahigh vacuum MBE system with a base pressure of $\sim 1.0 \times 10^{-10}$ Torr. The BLG/SiC substrate was prepared by vacuum annealing.[18,19] High-purity W (99.95%) was evaporated from an e-beam evaporator, and In (99.999%) and Se (99.999%) were evaporated from Knudsen cells. The flux ratios of W: Se and In: Se were 1:20. The substrate was kept at 750 K for the growth of WSe_2 and 560 K for the growth of In_2Se_3. The deposition of WSe_2 was followed by a 30 min annealing at the growth temperature with the Se flux maintained. The lateral HS was transferred into the STM chamber after naturally cooling to room temperature. The STM/STS measurements were performed by a commercial Unisoku 1400 system at 77 K (base pressure $< 1 \times 10^{-10}$ Torr). Electrochemically etched W-tips were used in all measurements. Constant Z differential conduction $(\mathrm{d}I/\mathrm{d}V)$ was taken by using a standard lock-in amplifier with a modulation voltage of 8 mV at a frequency of 932 Hz.

3. Results and discussion

Figure 1(a) shows the typical morphology of the ML-In_2Se_3–ML-WSe_2 lateral HS. A schematic of this lateral HS is displayed in Fig. 1(c). The apparent heights of ML In_2Se_3 and WSe_2 were measured as ~ 1.1 nm and ~ 0.8 nm, respectively (Fig. 1(b)). We observed two In_2Se_3 low-temperature phases as reported in the literature,[20,21] one was β'-In_2Se_3 with in-plane antiferroelectricity, and the other was β^*-In_2Se_3 with in-plane ferroelectricity. Figures 1(d) and 1(e) show the atomically resolved images of the β' and β^* phases. β'-In_2Se_3 had a one-dimensional reconstructed structure. Along the direction perpendicular to the [010] direction, the reconstruction period of the atomic lattice was eight or nine times larger.[21] The atomically resolved STM image showed that the stripe was formed by three or four rows of alternating Se atoms (with stronger contrast) and one row of Se atoms (with weaker contrast), and the stripe width was about 1.6 nm. In the stripe, Se atoms formed a hexagonal lattice with a lattice constant of about 0.40 nm. The β^* phase showed a basic hexagonal lattice with a surface Se atom lattice constant of about 0.40 nm and had a rectangular superlattice with a $2 \times \sqrt{3}$ surface reconstruction ($|\boldsymbol{a}_1| \approx 0.8$ nm, $|\boldsymbol{b}_1| \approx 0.7$ nm).[20,21]

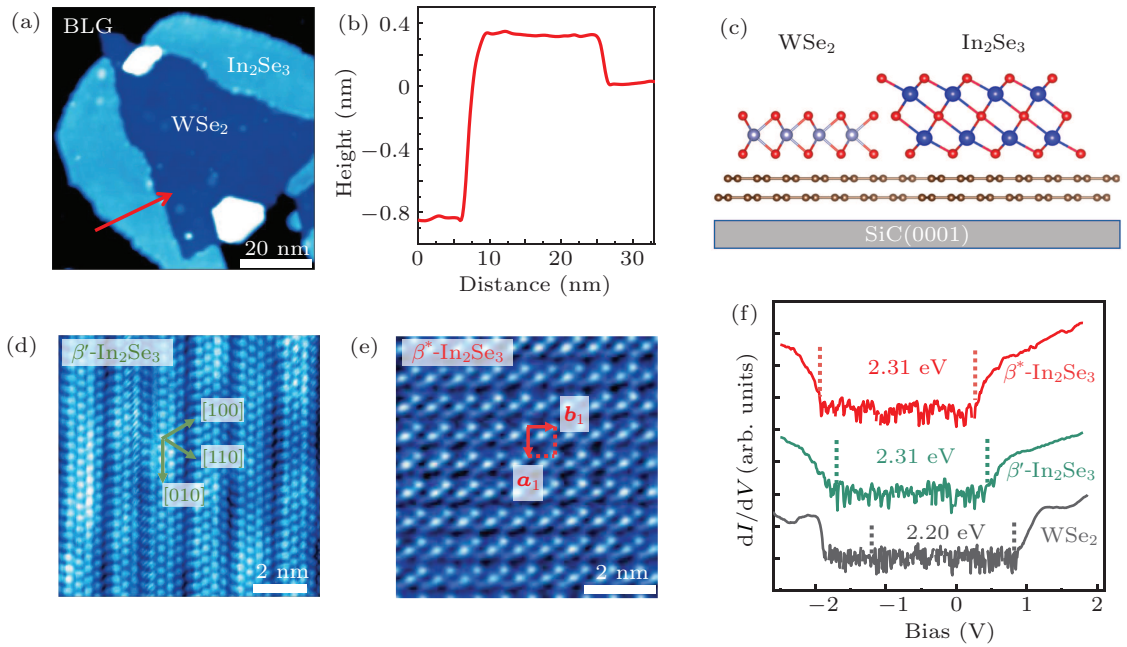


Fig. 1. (a) STM morphology of the ML-In_2Se_3–ML-WSe_2 lateral HS. Scanning parameters: bias voltage $V_{\mathrm{bias}} = 3$ V, tunneling current $I_{\mathrm{t}} = 10$ pA. (b) Line profile taken along the red line in (a). (c) Side view schematic of the lateral HS. The red, blue, gray, and brown spheres represent Se, In, W, and C atoms, respectively. (d), (e) Atomically resolved STM images of the β'-In_2Se_3 and β^*-In_2Se_3 phases. Scanning parameters: (d) $V_{\mathrm{bias}} = 600$ mV, $I_{\mathrm{t}} = 10$ pA, (e) $V_{\mathrm{bias}} = 500$ mV, $I_{\mathrm{t}} = 10$ pA. (f) Logarithm of $\mathrm{d}I/\mathrm{d}V$ spectra recorded over ML-β^*-In_2Se_3, ML-β'-In_2Se_3 and ML-WSe_2. The dashed lines indicate the valence band maximum (VBM) and conduction band minimum (CBM). Set point: $V_{\mathrm{bias}} = -2.5$ V, $I_{\mathrm{t}} = 100$ pA.

The tunneling conductance $(\mathrm{d}I/\mathrm{d}V)$ spectroscopy revealed that both phases of the ML-In_2Se_3 (on ML-WSe_2) were semiconductors with almost the same band gaps of 2.31 eV.[20] The critical point energy locations of WSe_2 were determined (marked in Fig. 1(f)) by variable Z spectroscopy [supporting information (SI) Fig. S1]. [21,22] The variable Z spectroscopy was taken at a constant tunneling current with the feedback loop on. This method could significantly enhance the dynamic

range, in which the tunneling barrier width was regulated according to the sweep of the bias. Therefore, type-II band alignments of the HSs formed by β^*/β' ML-In_2Se_3 and ML-WSe_2 were observed. Furthermore, the β^* phase exhibited a rigid upward shift of 0.2 eV compared to the β' phase, which was mainly due to the difference between their work functions.[21]

Figure 2(a) is the close-up STM image showing the lateral HS between ML WSe_2 and antiferroelectricity ML β'-In_2Se_3, a quasi-one-dimensional disordered structure appeared at the interface between WSe_2 and In_2Se_3 (SI Fig. S2). This may be caused by the different atomic layers of WSe_2 and In_2Se_3 which constituted the lateral HS. STS $(\mathrm{d}I/\mathrm{d}V)$ mapping was performed to study the electronic structure variations across the interface of the lateral HS. Figure 2(b) is a color rendering of the band mapping result taken along the red arrow in Fig. 2(a), and selected individual spectra are shown in Fig. 2(c). The numbers on the spectra referred to their positions in the complete set.

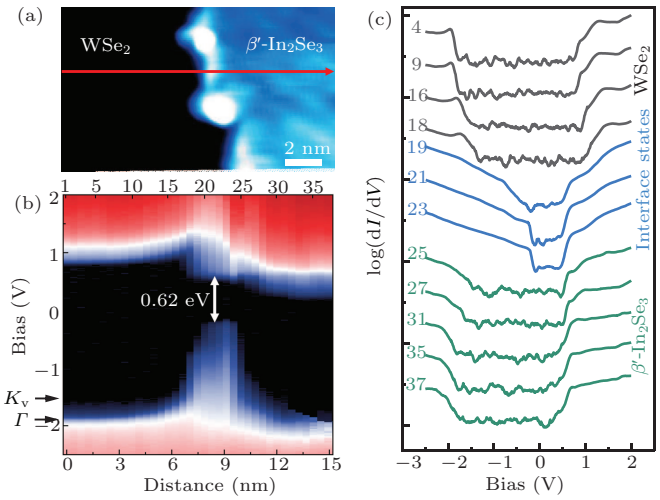


Fig. 2. (a) Topography image of β'-In_2Se_3–WSe_2 lateral HS. (b) Color-coded rendering of the real space imaging of the band profile plotted in terms of $\log(\mathrm{d}I/\mathrm{d}V)$. The $\mathrm{d}I/\mathrm{d}V$ spectra were taken along the path shown by the red arrow in (a). The bandgap of the interface is marked by the white arrow. (c) A selective subset of $\log(\mathrm{d}I/\mathrm{d}V)$ spectra. The spectra taken on WSe_2, interface, and β'-In_2Se_3 are represented by black, blue, and green, respectively. Set point: $V_{\mathrm{bias}} = 2$ V, $I_{\mathrm{t}} = 100$ pA.

The exception feature in Fig. 2(b) was the apparent upward band bending for both the conduction band and valence band of the ML WSe_2 and ML β'-In_2Se_3 regions near the interface. As reported in the literature, the edge of bare ML WSe_2 had upward band bending (SI Fig. S3), possibly due to the distribution of localized states,[23] and its magnitude was similar to the band bending of the edge of WSe_2 near the interface in Fig. 2(a). β'-In_2Se_3 had in-plane antiferroelectricity, all edges in β'-In_2Se_3 were considered neutral (SI Fig. S3), [20,21] whereas an obvious band bending occurred in the β'-In_2Se_3 region. The magnitude of the band bending in β'-In_2Se_3 was about 0.26 eV over about 2 nm toward the interface (depletion length). This could be attributed to the interfacial charge transfer (from interface to In_2Se_3). In addition, an abrupt change in the band structure right at the lateral HS interface could also be seen (see also spectra #19, #21, and #23 in Fig. 2(c)), as revealed by STS, the interface state behaved like a narrow gap semiconductor with a gap of 0.62 $\pm$0.08 eV. The $\mathrm{d}I/\mathrm{d}V$ map indicated that the interface states had type-I band alignment with both ML-WSe_2 and ML-β'-In_2Se_3 therefore can play the role of quantum wires for electrons and holes.[6]

At the LN_2 temperature, β'-In_2Se_3 was the most favored phase,[21] but there also existed a small amount of β^*-In_2Se_3. Figure 3(a) shows the topography image of β^*-In_2Se_3–WSe_2 lateral HS. Similar to the β'-In_2Se_3–WSe_2 lateral HS, there was also a quasi-one-dimensional disorder structure at the interface. The $\mathrm{d}I/\mathrm{d}V$ map (Fig. 3(b)) taken along the red arrow in Fig. 3(a) showed that WSe_2 had the same upward band bending as in Fig. 2(b). On the ML-β^*-In_2Se_3 region, there existed an upward band bending with a magnitude of about 0.51 eV and a depletion length of about 5 nm on approaching the interface. For materials with in-plane ferroelectricity, the edges with negative/positive charges would have upward/downward band bending,[14] so the edge of β^*-In_2Se_3 near the interface accumulated negative charges. The edge with negative charges of bare β^*-In_2Se_3 had an upward band bending with a magnitude of about 0.45 eV which was smaller than that of the edge with negative charges near the interface (SI Fig. S3). This was also the result of interfacial charge transfer, which increased the negative charges accumulated at the edge near the interface.

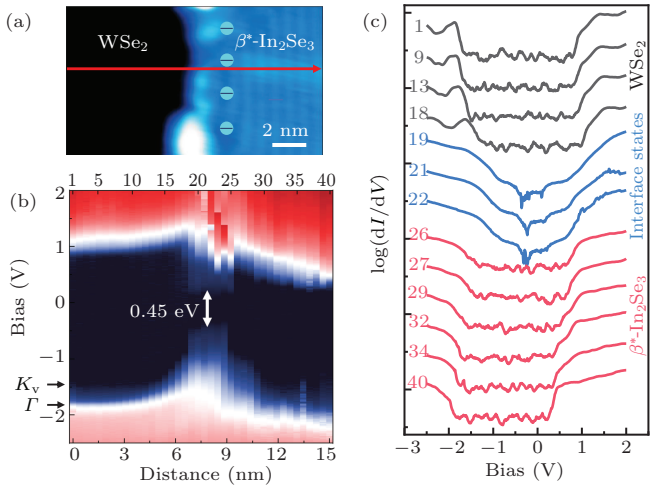


Fig. 3. (a) Topography image of β^*-In_2Se_3–WSe_2 lateral HS. The "–" symbols indicate the negative charges that accumulated on the edge of the β^*-In_2Se_3. (b) Color-coded rendering of the real space imaging of the band profile plotted in terms of $\log(\mathrm{d}I/\mathrm{d}V)$. The $\mathrm{d}I/\mathrm{d}V$ spectra were taken along the path shown by the red arrow in (a). The bandgap of the interface is marked by the white arrow. (c) A selective subset of $\log(\mathrm{d}I/\mathrm{d}V)$ spectra. The spectra taken on WSe_2, interface, and β^*-In_2Se_3 are represented by black, blue, and red, respectively. Set point: $V_{\mathrm{bias}} = 2$ V, $I_{\mathrm{t}} = 100$ pA.

An exceptional feature of electronic structures was also observed at the β^*-In_2Se_3–WSe_2 lateral HS interface (Fig. 3(b)). Similar to the features in β'-In_2Se_3–WSe_2 lateral

HS, the interface in β^*-In_2Se_3–WSe_2 lateral HS also had type-I band alignment with both ML-WSe_2 and ML-β^*-In_2Se_3. However, the selective individual dI/dV spectra (#19, #21, and #22) in Fig. 3(c) revealed that the interface state in β^*-In_2Se_3–WSe_2 lateral HS had a band gap of about 0.45 eV, which was smaller than that in β'-In_2Se_3–WSe_2 lateral HS.

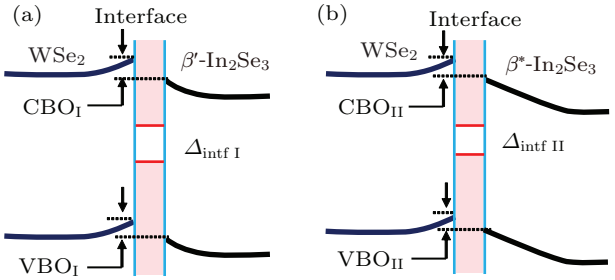


Fig. 4. Schematic diagram of band alignment in β'-In_2Se_3–WSe_2 lateral HS (a) and β^*-In_2Se_3–WSe_2 lateral HS (b). The band gaps of interface states in β'-In_2Se_3–WSe_2 lateral HS and β^*-In_2Se_3–WSe_2 lateral HS are labeled as $\Delta_{\text{intf I}}$ and $\Delta_{\text{intf II}}$, respectively.

We summarized the general features of lateral HSs formed from WSe_2 and β'-In_2Se_3 or β^*-In_2Se_3 with the schematic diagram (Figs. 4(a) and 4(b)). Here, the conduction band offset was labeled as CBO, the valence band offset as VBO and the gap of the interface was labeled as Δ_{intf}. The values for these quantities are summarized in Table 1 for β'-In_2Se_3–WSe_2 lateral HS and β^*-In_2Se_3–WSe_2 lateral HS, respectively. We also used constant current spectroscopy to detect the critical point energy location in the valence band (labeled as K_v and Γ in Figs. 2(b) and 3(b)) of ML-WSe_2 (SI Fig. S1). The VBM of ML-WSe_2 was located at the K_v point, about 0.60 eV above the Γ point. With this information, we determined that the CBO_I and VOB_I of β'-In_2Se_3–WSe_2 HS were 0.40±0.10 eV and 0.15±0.05 eV, respectively. Similarly, the COB_{II} and VOB_{II} of β^*-In_2Se_3–WSe_2 HS were 0.30±0.10 eV and 0.10±0.05 eV, respectively. The CBO and VBO in β^*-In_2Se_3–WSe_2 HS were smaller than those in β'-In_2Se_3–WSe_2, and the maximum difference was 100 meV, which may be due to the greater upward band bending of β^*-In_2Se_3 caused by the ferroelectric polarization. In addition, in both systems, a narrow gap quantum wire existed at the interface. The interface state in β'-In_2Se_3–WSe_2 lateral HS had a gap $\Delta_{\text{intf I}}$ of about 0.62±0.10 eV. Similarly, the gap $\Delta_{\text{intf II}}$ of the interface state in β^*-In_2Se_3–WSe_2 lateral HS reduced to 0.45±0.05 eV. In the previous literature,[24–26] some research teams modulated the band gap of one-dimensional systems such as nanotubes and nanoribbons by applying an external transverse electric field. Therefore, in our system, the ferroelectric polarization in β^*-In_2Se_3 was also a factor that could not be ruled out to affect the band gap of the interface states. Interestingly, we investigated several β^*-In_2Se_3 lateral HS, but only negatively charged edges of β^*-In_2Se_3 were observed near the interface. This might be because, in the process of forming lateral HS, the negatively charged edge of β^*-In_2Se_3 was preferred to form the interface with WSe_2. The preferred polarization direction at the interface of a 2D ferroelectric lateral HS had also been reported in previous research.[5]

Table 1. Band alignments in lateral HSs.

HS	CBO (eV)	VBO (eV)	Δ_{intf} (eV)
β'-In_2Se_3–WSe_2	0.40±0.10	0.15±0.05	0.62±0.10
β^*-In_2Se_3–WSe_2	0.30±0.10	0.1±0.05	0.45±0.10

4. Conclusion

We successfully fabricated the lateral HS with three atomic layers of ML WSe_2 and five atomic layers of ML In_2Se_3 by a two-step MBE process. We measured the band profile using STM/S and visualized the spatial evolution of electronic structures. We observed that the CBO and VBO of HS could be modulated by ferroelectric polarization, with a maximum difference of 100 meV. In particular, we demonstrated that the interface states in both lateral HSs form a narrow gap quantum wire which had type-I band alignment with both WSe_2 and In_2Se_3. The band gap of the interface state in β'-In_2Se_3–WSe_2 lateral HS was about 0.62 eV, which was larger than 0.45 eV in β^*-In_2Se_3–WSe_2 lateral HS, where the ferroelectric polarization of β^*-In_2Se_3 was a reason that could not be ruled out. We expect that the fabrication of this ferroelectric lateral HS and the modulation of interface electronic states will contribute to the development of 2D ferroelectric devices.

Acknowledgements

Project supported by the National Key R&D Program of China (Grant Nos. 2018YFA0305800 and 2018YFA0703700), the National Natural Science Foundation of China (Grant Nos. 11974012 and 12134011), and the Strategic Priority Research Program of Chinese Academy of Sciences (Grant No. XDB3000000).

References

[1] Marin E G, Marian D, Perucchini M, Fiori G and Iannaccone G 2020 *ACS Nano* **14** 1982
[2] Zhao Y, Guo F, Ding R, Io W F, Pang S Y, Wu W and Hao J 2021 *Adv. Opt. Mater.* **9** 2100864
[3] Sup Choi M, Lee G H, Yu Y J, Lee D Y, Lee S H, Kim P, Hone J and Yoo W J 2013 *Nat. Commun.* **4** 1624
[4] Gong Y, Lin J, Wang X, Shi G, Lei S, Lin Z, Zou X, Ye G, Vajtai R and Yakobson B I 2014 *Nat. Mater.* **13** 1135
[5] Chang K, Villanova J W D, Ji J R, Das S, Kuster F, Barraza-Lopez S, Sessi P and Parkin S S P 2021 *Adv. Mater.* **33** 2102267
[6] Zhang C, Chen Y, Huang J K, Wu X, Li L J, Yao W, Tersoff J and Shih C K 2016 *Nat. Commun.* **7** 10349
[7] Duan X, Wang C, Shaw J C, Cheng R, Chen Y, Li H, Wu X, Tang Y, Zhang Q and Pan A 2014 *Nat. Nanotech.* **9** 1024
[8] Zhang C, Li M Y, Tersoff J, Han Y, Su Y, Li L J, Muller D A and Shih C K 2018 *Nat. Nanotech.* **13** 152
[9] Ling X, Lin Y, Ma Q, Wang Z, Song Y, Yu L, Huang S, Fang W, Zhang X and Hsu A L 2016 *Adv. Mater.* **28** 2322

[10] Zhao M, Ye Y, Han Y, Xia Y, Zhu H, Wang S, Wang Y, Muller D A and Zhang X 2016 *Nat. Nanotech.* **11** 954
[11] Hong W, Shim G W, Yang S Y, Jung D Y and Choi S Y 2018 *Adv. Funct. Mater.* **29** 1807550
[12] Deng W, Chen Y, You C, Liu B, Yang Y, Shen G, Li S, Sun L, Zhang Y and Yan H 2018 *Adv. Electron. Mater.* **4** 1800069
[13] Ding W, Zhu J, Wang Z, Gao Y, Xiao D, Gu Y, Zhang Z and Zhu W 2017 *Nat. Commun.* **8** 14956
[14] Chang K, Liu J, Lin H, Wang N, Zhao K, Zhang A, Jin F, Zhong Y, Hu X and Duan W 2016 *Science* **353** 274
[15] Si M, Liao P Y, Qiu G, Duan Y and Ye P D 2018 *ACS Nano* **12** 6700
[16] Jin H J, Park C, Lee K J, Shin G H and Choi S Y 2021 *Adv. Mater. Technol.* **6** 2100494
[17] Zhang Q, Hou Y, Zhang T, Xu Z, Huang Z, Yuan P, Jia L, Yang H, Huang Y and Ji W 2021 *ACS Nano* **15** 16589
[18] Wang Q, Zhang W, Wang L, He K, Ma X and Xue Q 2013 *J. Phys.: Condens. Matter* **25** 095002
[19] Brar V W, Zhang Y, Yayon Y, Ohta T, McChesney J L, Bostwick A, Rotenberg E, Horn K and Crommie M F 2007 *Appl. Phys. Lett.* **91** 122102
[20] Zhang Z, Nie J, Zhang Z, Yuan Y, Fu Y S and Zhang W 2022 *Adv. Mater.* **34** 2106951
[21] Huo D, Bai Y, Lin X, Deng J, Pan Z, Zhu C, Liu C, Yu H and Zhang C 2022 *Nano Lett.* **22** 7261
[22] Zhang C, Chen Y, Johnson A, Li M Y, Li L J, Mende P C, Feenstra R M and Shih C K 2015 *Nano Lett.* **15** 6494
[23] Le Quang T, Nogajewski K, Potemski M, Dau M T, Jamet M, Mallet P and Veuillen J Y 2018 *2D Mater.* **5** 035034
[24] Dolui K, Pemmaraju C D and Sanvito S 2012 *ACS Nano* **6** 4823
[25] Ishigami M, Sau J D, Aloni S, Cohen M L and Zettl A 2005 *Phys. Rev. Lett.* **94** 056804
[26] Zheng F, Liu Z, Wu J, Duan W and Gu B L 2008 *Phys. Rev. B* **78** 085423